

Moisture Effects on Conduction Loads

N. Mendes¹
Pontifical Catholic
University of Paraná
Department of Mechanical
Engineering
Thermal Systems Laboratory
Curitiba-PR
80.215-901
Brazil

F. C. Winkelmann
Lawrence Berkeley National
Laboratory
Environmental Energy
Technologies Division
Simulation Research Group
Berkeley – CA, 94720
USA

R. Lamberts
Federal University of Santa
Catarina
Florianópolis-SC
88.040-900
Brazil

P.C. Philippi
Federal University of Santa
Catarina
Florianópolis-SC
88.040-900
Brazil

ABSTRACT	1
1 INTRODUCTION	1
2 MATHEMATICAL MODEL	2
3 SIMULATION PROCEDURE	5
3.1 Indoor air temperature and relative humidity prediction	5
3.2 Material Properties	7
4 RESULTS AND DISCUSSION	9
4.1 Sensitivity of CPL and YHF to the terms in the heat and moisture transfer mode	9
4.2 Influence of temperature gradients on moisture diffusion	13
4.3 Paint layer effects	14
5 CONCLUSIONS	18
ACKNOWLEDGMENTS	19
NOMENCLATURE	19
REFERENCES	20
LIST OF TABLES	21
LIST OF FIGURES	21

¹ Corresponding author. Tel.: +55-41-330-1322; fax: +55-41-330-1349.

E-mail address: nmendes@ccet.pucpr.br (N. Mendes)

Moisture Effects on Conduction Loads

N. Mendes^{a,2}, F. C. Winkelmann^b, R. Lamberts^c and P.C. Philippi^c

^a Pontifical Catholic University of Paraná, Department of Mechanical Engineering, Thermal Systems Laboratory, Curitiba-PR, 80.215-901, Brazil

^b Lawrence Berkeley National Laboratory, Environmental Energy Technologies Division, Simulation Research Group, Berkeley – CA, 94720, USA

^c Federal University of Santa Catarina, Florianópolis-SC, 88.040-900, Brazil

ABSTRACT

The effects of moisture on sensible and latent conduction loads are shown by using a heat and mass transfer model with variable material properties, under varying boundary conditions. This model was then simplified to reduce calculation time and used to predict conduction peak load and yearly integrated wall conduction heat flux in three different cities: Singapore (hot/humid), Seattle (cold/humid) and Phoenix (hot/dry). The room air temperature and relative humidity were calculated with the building energy simulation program DOE-2.1E. The materials studied were aerated cellular concrete, brick, lime mortar and wood. It is shown that the effects of moisture can be very significant and that simplified mathematical models can reduce the calculation time with varying effects on accuracy.

1 INTRODUCTION

In building energy analysis the calculation of heat conduction through walls usually neglects the storage and transport of moisture in the porous structure of the walls. However, walls are normally subjected to both thermal and moisture gradients so that an accurate heat transfer determination requires a simultaneous calculation of both sensible and latent effects. The transfer of moisture through common building materials, such as wood, concrete and brick, depends on the complex morphotopological characteristics of the pores in these materials. Therefore, it is important to consider hygroscopic phenomena in building energy simulation; however, this usually implies much longer run times.

Several investigators have developed models for moisture transport in buildings [1-6]. Some models use the response factor method so that they are limited to constant transport coefficients. Others are limited to low moisture content. Lacking a data base of moisture transport coefficients and faced with long run times, we have developed a faster-running model that is dynamic but avoids restrictions such as low moisture content and constant transport coefficients.

In the work of International Energy Agency Annex 24 [7], five programs were presented in detail: 1D-HAM, WUFIZ, MATCH, HYGRAN24 and LATENITE. All of these programs have a similar physical basis: heat and mass balance equations, Philip and De Vries model, and the laws of Fourier, Fick and Darcy. The main difference among the programs are the simplifying assumptions that are made. Some models, such as that used in MOIST, have been validated for some cases and shown to be reliable [8-9]. Therefore, it is believed that these models are generally reliable, especially for weather conditions that are not too humid.

Our dynamic model allows the cooling loads due to combined heat and moisture transport through walls to be calculated for a wide range of materials, even under the extreme conditions found in hot/humid climates. For the walls we consider sensible and latent surface convection, absorbed solar radiation, heat and mass transfer through the wall, and vapor/liquid phase change. The walls are described mathematically using the model of Philip and DeVries [10] in which vapor and liquid flow under moisture and thermal gradients and the mathematical model used was the same proposed by Mendes et al. [11]. In this model, heat, vapor and liquid flow are taken to be simultaneous and coupled. Physical quantities, such as mass transport coefficients, thermal conductivity and specific heat, are variable and depend on wall temperature and moisture content. We have created submodels from this model by making various simplifications, such as assuming constant coefficients, neglecting latent effects within the wall, working with both “pure” and “apparent” thermal conductivity and approaching, in

² Corresponding author. Tel.: +55-41-330-1322; fax: +55-41-330-1349

E-mail address: nmendes@ccet.pucpr.br (N. Mendes)

the most simplified form, Fourier's equation for transient heat flow. From these submodels we can determine how the simplifications effect accuracy and run time.

Submodel analysis is done for four different types of wall material: aerated cellular concrete, brick, lime mortar and wood. For the simulations we used Typical Meteorological Year (TMY) weather files for three different climates: Singapore (Hot/Humid), Seattle (Cold/Humid) and Phoenix (Hot/Dry). Hourly room air temperature and relative humidity were calculated with the DOE-2.1E building energy simulation program [12-13]. The submodels are compared to the results of the original, unsimplified model to determine the effect on cooling loads and simulation run time.

We also present results showing the importance of the terms in the heat and mass transfer model and the influence of weather on the conduction loads. In most cases, we shall see that simplified heat and moisture transfer models lead to acceptable results, while at the same time reducing the run time and number of inputs.

2 MATHEMATICAL MODEL

The governing partial differential equations to model heat and mass transfer through porous walls are given by equations (1) and (2). They were derived from conservation of mass and energy flow in a 1-D elemental volume of porous material, since the temperature and moisture content gradients are predominantly in the x direction. Therefore, the energy conservation equation is written as

$$\rho_0 c_m(T, \theta) \frac{\partial T}{\partial t} = \frac{\partial}{\partial x} (\lambda(T, \theta) \frac{\partial T}{\partial x}) - L(T) \frac{\partial}{\partial x} (j_v) \quad (1)$$

and the mass conservation equation as

$$\frac{\partial \theta}{\partial t} = - \frac{\partial}{\partial x} \left(\frac{j}{\rho_1} \right) \quad (2)$$

Note that eq. (1) differs from Fourier's equation for transient heat flow by an added convective transport term (due to moisture diffusion associated with evaporation and condensation of water in the pores of the medium) and by a dependence on the moisture content (so that it is coupled to eq. (2)). The driving forces for convective transport are temperature and moisture gradients. The vapor flow (J_v) and total flow (J - vapor plus liquid) are expressed in terms of transport coefficients, D , associated with the thermal and moisture gradients [10] as:

$$\frac{j_v}{\rho_1} = -D_{T_v}(T, \theta) \frac{\partial T}{\partial x} - D_{\theta_v}(T, \theta) \frac{\partial \theta}{\partial x}; \quad (3)$$

$$\frac{j}{\rho_1} = -D_T(T, \theta) \frac{\partial T}{\partial x} - D_\theta(T, \theta) \frac{\partial \theta}{\partial x} \quad (4)$$

Internally, the wall is exposed to convection and phase change and externally ($x=0$) it is exposed to solar radiation (αq_r), convection $h_{ext}(T_{ext} - T(0))$ and phase change ($h_{m,ext}(\rho_{v,ext} - \rho_{v,x=0})$), so that the energy equation becomes

$$-\left(\lambda(T,\theta)\frac{\partial T}{\partial x}\right)_{x=0} - (L(T)j_v)_{x=0} = h_{\text{ext}}(T_{\text{ext}} - T_{x=0}) + \alpha q_r + L(T)h_{m,\text{ext}}(\rho_{v,\text{ext}} - \rho_{v,x=0}). \quad (5)$$

where h ($T_{\infty} - T_{x=0}$) represents the heat exchanged with the outside air (described by the surface conductance h), αq_r is the absorbed short-wave radiation, and $h_m(\rho_{v,\infty} - \rho_{v,x=0})$ is the phase-change energy term. The solar absorptivity is α and the mass convection coefficient is h_m , which is related to h by the Lewis relation.

The mass balance at the outside surface ($x=0$) is

$$-\frac{\partial}{\partial x}(D_{\theta}(T,\theta)\frac{\partial \theta}{\partial x} + D_T(T,\theta)\frac{\partial T}{\partial x})_{x=0} = \frac{h_m}{\rho_l}(\rho_{v,\infty} - \rho_{v,x=0}). \quad (6)$$

The above equations also apply to the inside surface ($x=L$), with the omission of short-wave related terms.

Submodels

In order to reduce CPU time or when there is a lack of material data, we derived six submodels as follows:

$$\rho_0 c_m(T,\theta)\frac{\partial T}{\partial t} = \frac{\partial}{\partial x}(\lambda(T,\theta)\frac{\partial T}{\partial x}) + L(T)\rho_l\frac{\partial}{\partial x}\left(D_{Tv}(T,\theta)\frac{\partial T}{\partial x}\right) + L(T)\rho_l\frac{\partial}{\partial x}\left(D_{\theta v}(T,\theta)\frac{\partial \theta}{\partial x}\right). \quad (7)$$

To simplify writing this equation, we will use V_T and V_{θ} to designate the second and third right-hand terms of eq. (7):

$$V_T = L(T)\rho_l\frac{\partial}{\partial x}\left(D_{Tv}(T,\theta)\frac{\partial T}{\partial x}\right)$$

$$V_{\theta} = L(T)\rho_l\frac{\partial}{\partial x}\left(D_{\theta v}(T,\theta)\frac{\partial \theta}{\partial x}\right)$$

Therefore, Eq. (7) can be rewritten as

$$\rho_0 c_m(T,\theta)\frac{\partial T}{\partial t} = \frac{\partial}{\partial x}\left(\lambda(T,\theta)\frac{\partial T}{\partial x}\right) + V_T + V_{\theta}. \quad (8)$$

Submodel 0 is the same as the original model given by Eqs. (1-6). Submodel 1 omits the source term in Eq. (8), which is associated with a moisture gradient (V_{θ}). In this case, the equation resulting from Eq. (8) can also be written as a function of the λ_{app} as:

$$\rho_0 c_m(T,\theta)\frac{\partial T}{\partial t} = \frac{\partial}{\partial x}(\lambda_{\text{app}}(T,\theta)\frac{\partial T}{\partial x}), \quad (9)$$

where the ‘‘apparent’’ thermal conductivity (λ_{app}) is related to the ‘‘pure’’ thermal conductivity, λ , by the following expression:

$$\lambda_{\text{app}}(T,\theta) = \lambda(T,\theta) + L(T)\rho_l D_{Tv}(T,\theta). \quad (10)$$

Therefore, Submodel 1 is obtained by combining Eqs. (2-6) and Eqs. (9-10).

Now, if we disregard the other source term (V_T) in Eq. (8), we obtain Submodel 2 by transforming eq. (9) to:

$$\rho_0 c_m(\tau, \theta) \frac{\partial T}{\partial t} = \frac{\partial}{\partial x} \left(\lambda(\tau, \theta) \frac{\partial T}{\partial x} \right). \quad (11)$$

Submodel 3 is the same as Submodel 2, except that the pure thermal conductivity, λ , is constant so that Eq. (11) for Submodel 3 can be written as:

$$\rho_0 c_m(\tau, \theta) \frac{\partial T}{\partial t} = \lambda \frac{\partial^2 T}{\partial x^2}. \quad (12)$$

In Submodel 4, the coefficients D_θ , D_T and λ and the specific heat are held constant. Therefore, for Submodel 4, the energy and mass conservation equations can be written as:

$$\rho_0 c_m \frac{\partial T}{\partial t} = \lambda \frac{\partial^2 T}{\partial x^2}, \quad (13)$$

$$\frac{\partial \theta}{\partial t} = D_T(\tau, \theta) \frac{\partial^2 T}{\partial x^2} + D_\theta(\tau, \theta) \frac{\partial^2 \theta}{\partial x^2}. \quad (14)$$

In fact, all of the submodels have the same basic mathematical structure except for Submodel 5 which neglects all moisture effects. In Submodel 5, the governing equation is the Fourier's equation for transient heat flow with constant thermophysical properties, as described in Eq. (13). However, the boundary conditions are written as

$$-\left(\lambda \frac{\partial T}{\partial x} \right)_{x=0} = h_{\text{ext}}(T_{\text{ext}} - T_{x=0}) + \alpha q_r. \quad (15)$$

Table 1 summarizes the submodels derived from the original model.

Table 1: Summary of the submodels.

Submodel	Assumptions
0	none (original model)
1	$V_\theta = 0$
2	$V_T, V_\theta = 0$
3	$V_T, V_\theta = 0$ and $\lambda = \text{constant}$.
4	$V_T, V_\theta = 0$ and D_T, D_θ, c_m and $\lambda = \text{constant}$
5	$D_\theta, D_T, D_{\theta V}, D_{TV} = 0$ and $c_m, \lambda = \text{constant}$

Submodel 0 is the most precise and, therefore, the most compute intensive. The accuracy of each submodel depends basically on the material properties and on the moisture content levels. For hygroscopic walls, for example, submodel simplifications can result in larger errors.

The mathematical treatment for the discontinuity on the moisture content profile is described by Mendes and Philippi [14].

3 SIMULATION PROCEDURE

The mathematical model was solved by using a finite-volume approach with a fully-implicit solution scheme and coupling between the governing equations. Using the Patankar method [15] with uniform nodal spacing and a new method to solve those highly-coupled equations [11], a C program solves temperature and moisture content distributions simultaneously at each 1-hour time step. Each case was pre-simulated with a one-year warm-up period to study vertical walls of lime mortar, brick, aerated cellular concrete and wood. The external convection coefficient was fixed at 12.4 W/m²K and the internal at 3.6 W/m²K. The mass convection coefficients were obtained by the Lewis relation, considering Lewis number equals to 1, which gives for the external and internal surfaces 0.01054 and 0.00306 m/s. The reflectance of the ground in front of the wall was ignored and the solar absorptivity of the external surface of the wall was 0.35.

3.1 Indoor air temperature and relative humidity prediction

Since the model does not do a whole-building energy analysis, the program DOE-2 was considered as a simulation engine to provide indoor air. In other words, we assumed that room air temperature and relative humidity would not be really affected if we could replace DOE-2 models by one of the Submodels 1-5.

Therefore, indoor air temperature and relative humidity were predicted for each of the three cities by using the hourly building simulation program DOE-2.1E for a room in the 2nd floor of a 8-story building. The air conditioning was turned on from 8am to 5pm on weekdays; on weekends and holidays it was turned off. The façade with the smallest solar irradiance was chosen in order to avoid high moisture losses by evaporation, representing a more critical situation. Therefore, in Phoenix and Seattle the room faced north, while in Singapore it faced south. There was a constant ventilation rate of 42.2 m³/h (0.13 ach⁻¹) between 8am and 5pm. At other times the ventilation rate was 30% of this value. Infiltration was assumed to produce an air flow of 1.8 m³/h for each square meter of external wall area.

Each room of the building has an area of 108 m² and a volume of 324 m³. The external wall has a total area of 36 m² (12 m² are glazed). The light and equipment power densities were assumed to be 29 W/m² and 6 W/m², respectively. Cooling was provided by a window air conditioner (PTAC system in DOE-2.1E). It is important to point out that DOE 2.1E was run independently of the heat and mass transfer models and was used only to calculate the room air temperature and relative humidity. The alternative of using constant conditions for the interior would hide, for example, the phenomenon of phase change, in which condensation occurs at night period and evaporation occurs during the day.

Figures 1-3 show some of the results. In Fig. 1 we note that the inside air temperature stays around the cooling set point of 23 °C when the air conditioning is on. However, during the night, this temperature increases to slightly above the outside air temperature. Similarly, the inside relative humidity increases at night and approaches the outside air value. It decreases when the air conditioning is turned on as shown in Fig. 2.

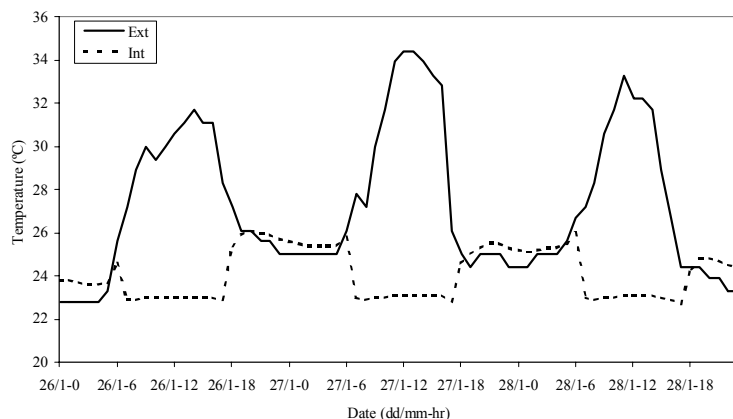


Figure 1: Internal and external temperatures in Singapore.

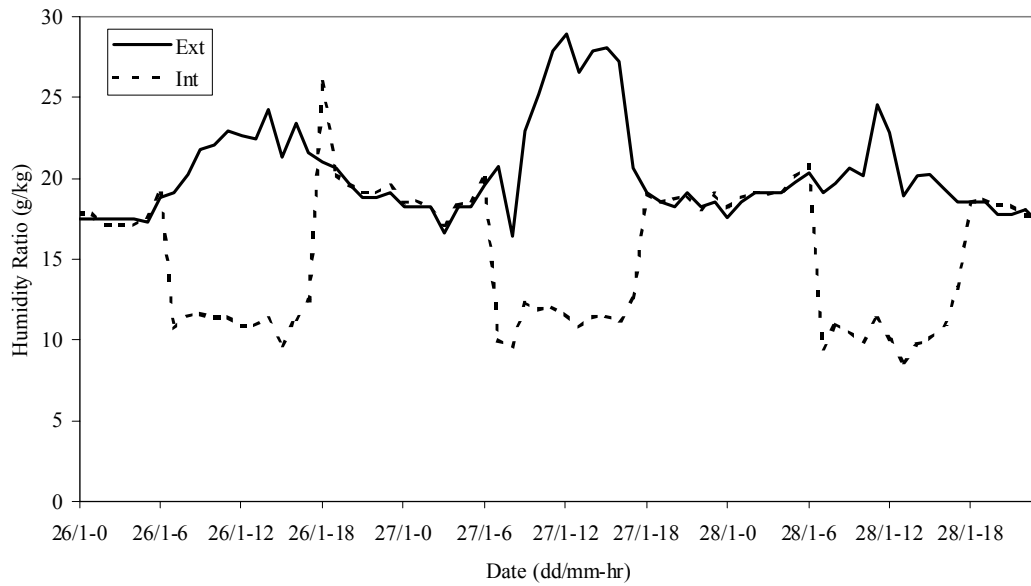


Figure 2: External and internal humidity ratios in Singapore.

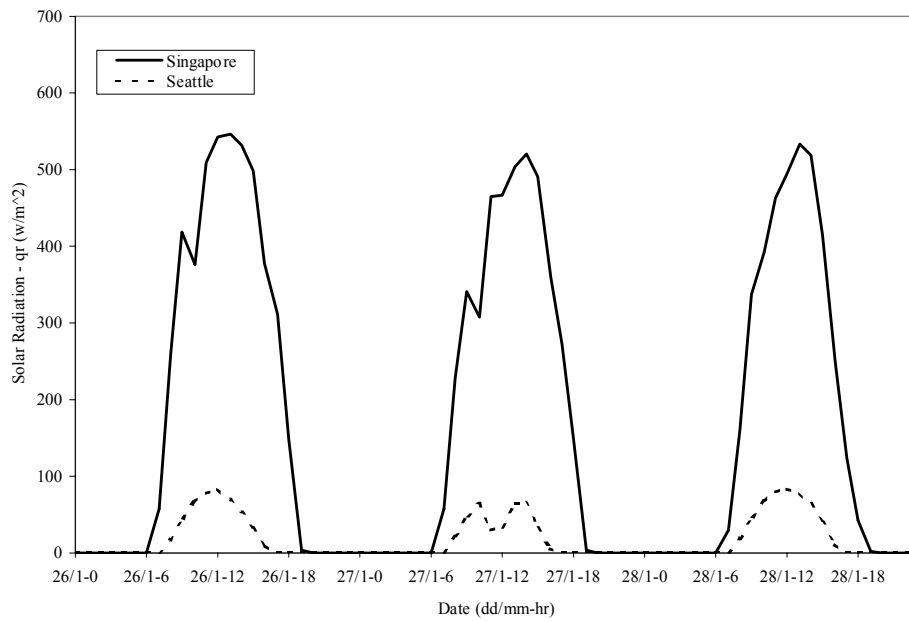


Figure 3: Incident solar radiation on the south facade for Singapore and on the north facade for Seattle.

Figure 3 shows the direct solar radiation incidence on the wall for Singapore (south wall) and Seattle (north wall). For the same period we see that the solar radiation in Singapore (summer) it is much larger than that in Seattle (winter), which is below 240 W/m² during the winter.

3.2 Material Properties

The basic dry-basis material properties are given in Table 2. Here, “open porosity” is the ratio of the volume of open pores (i.e., pores with openings that have a path to both wall surfaces) to the total volume.

Table 2: Dry-basis material properties for lime mortar.

Property	Brick	Mortar
ρ_0 [kg/m ³]	1900	2050
λ (W/m-K)	1.11	1.96
c [J/kg-K]	920	950
Open porosity	0.29	0.18

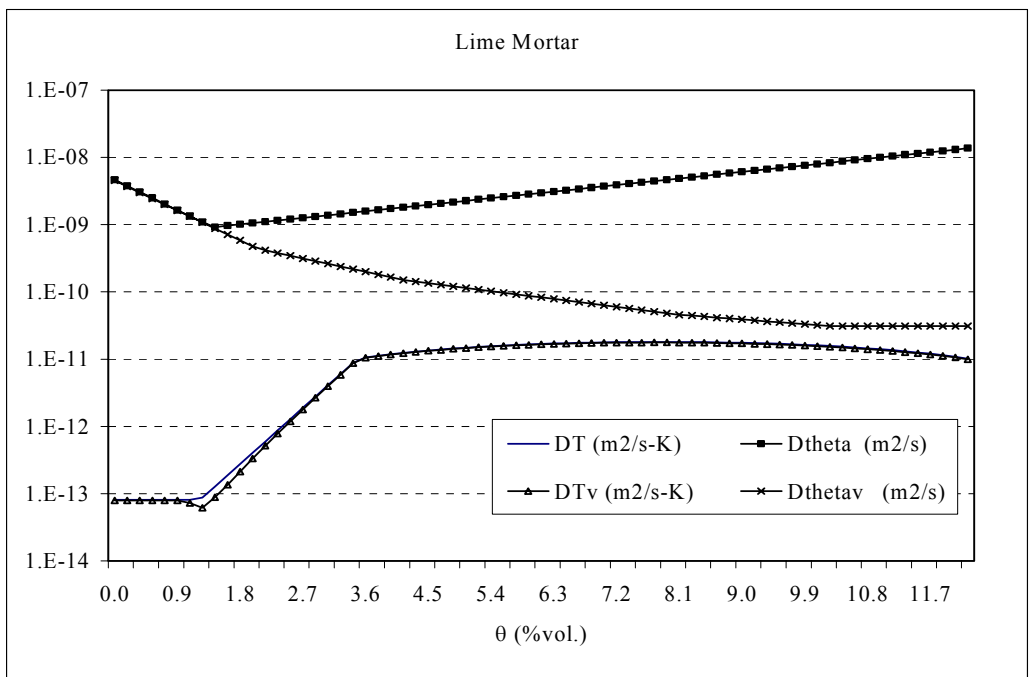


Figure 4: Mass transport coefficients for lime mortar

The available material data from Perrin [16] allows all the transport coefficients to be modeled as a function of moisture content. Figures 4-7 show the property data for both materials; however they are slightly different from those presented by Perrin because fitting coefficients were applied on his experimental data. Instead of recalculating all coefficients at each iteration, the program reads them from files which considerably speeds up simulations.

Figures 4 and 5 show vapor and total (liquid plus vapor) transport coefficients for lime mortar and brick. We see that the coefficient responsible for the flow of liquid due to a temperature gradient (D_{TL}) is very small compared to the one for vapor since the differences between the curves of D_T and D_{T_v} are very small.

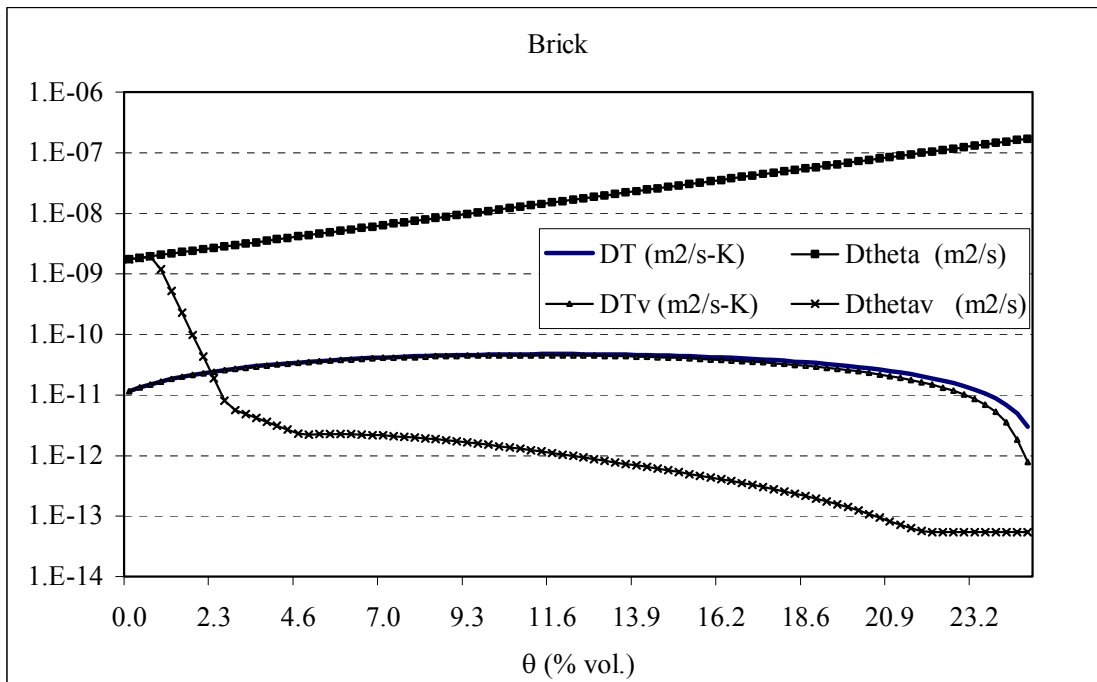


Figure 5: Mass transport coefficients for brick

Figure 6 shows the thermal conductivity curves for both materials. The vapor diffusion and phase change effects were not considered in these curves, which means that they show the value for pure thermal conduction according to Fourier's law.

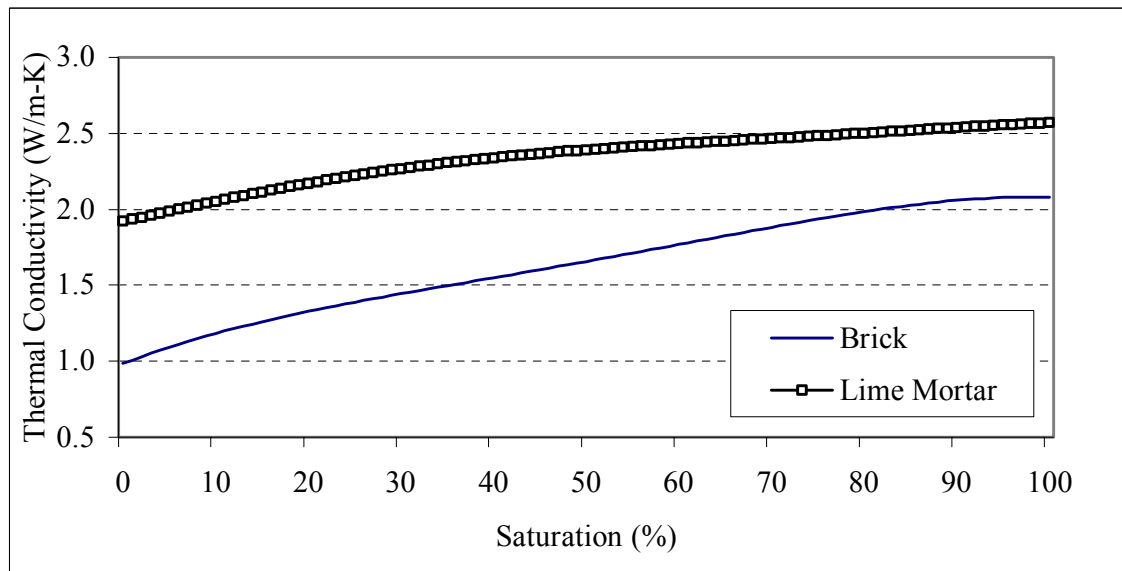


Figure 6: Thermal conductivity for brick and lime mortar.

These transport coefficients (thermal conductivity λ , vapor transport coefficients – D_{TV} , $D_{\theta V}$ - and liquid transport coefficients – D_{TL} , $D_{\theta L}$) are always evaluated between two consecutive grid nodes by a harmonic mean due to their high variation with moisture content.

Figure 7 shows the sorption isotherms for both materials. These curves are the average between adsorption and desorption curves. We see from this figure that lime mortar is more hygroscopic than brick. Material property data on wood can be found in [17] and on aerated cellular concrete in [18].

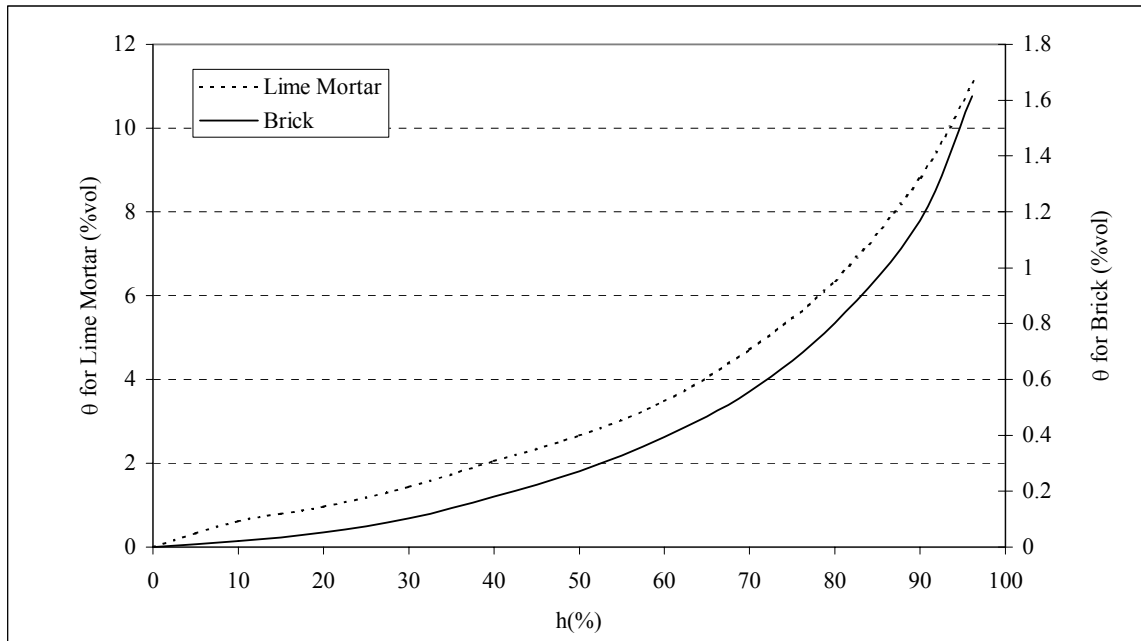


Figure 7: Sorption isotherms curves for brick and lime mortar.

4 RESULTS AND DISCUSSION

In this section, we show the effects on conduction peak load (CPL) and yearly-integrated conduction heat flux (YHF) through a wall. The simplifications were applied to formulation terms and material properties as shown in Section 2 to derive the six submodels described in Section 4.1. Four materials were studied: aerated cellular concrete (ACC), brick (BRK), lime mortar (LMT) and wood. In Section 4.2 we demonstrates the importance of temperature gradients in the moisture diffusion through building walls. Section 4.3 shows the effects of surface paint on the coupled heat and moisture transfer.

4.1 Sensitivity of CPL and YHF to the terms in the heat and moisture transfer mode

The full heat and mass transfer model presented includes all of the Philip and De Vries model terms. It assumes that all transport coefficients are variable with moisture content and temperature, making itself as a time consuming model, especially when the goal is to simulate an entire building. In order to verify the importance of simplifying assumptions, we present sensitivity analyses in terms of CPL and YHF. The study was carried out for two wall types: W1 (20mm lime mortar/100mm brick/20mm lime mortar) and W2 (50mm wood). Submodels 0 and 2 were not used for W2 since no data are available for the coefficients $D_{\theta V}$ and D_{TV} for wood.

Table 3: Conduction Peak Load (CPL), maximum latent heat factor $[Q_L/Q_T]_{CPL}$, peak load date/hour, Yearly-Integrated Conduction Heat Flux (YHF) and yearly latent heat factor $[Q_L/Q_T]_{YHF}$ for walls W1 (Submodel 0) and W2 (Submodel 1) in the 3 cities.

	W1			W2		
	Singapore	Seattle	Phoenix	Singapore	Seattle	Phoenix
CPL(W/m ²)	44.2	-107.5	44.4	86.7	-87.2	91.4
$[Q_L/Q_T]_{CPL}$	0.33	0.40	0.10	0.64	0.48	0.54
Date (d/m-h) _{CPL}	Jan. 27, 5pm	Dec. 6, 9am	Aug. 1, 5pm	Jan. 27, 3pm	Dec. 6, 9am	Aug. 2, 2pm
YHF (kWh/m ²)	23288	-76154	24397	47612	-64420	45319
$[Q_L/Q_T]_{YHF}$	0.62	0.22	0.28	0.57	0.34	0.44

Table 3 shows results for CPL and YHF for the walls W1 (Submodel 0) and W2 (Submodel 1) in the three cities. Note that loads are for cooling in Singapore and Phoenix, and for heating in Seattle. Table 4 shows estimation errors among different models.

Table 4: Conduction Peak Load (CPL) and Yearly-Integrated Conduction Heat Flux (YHF) estimation errors (in %) in Singapore, Seattle and Phoenix, compared to Submodel 0 (Submodel 1 for W2).

Wall	City	Submodel									
		1		2		3a		3b		3c	
		CPL	YHF	CPL	YHF	CPL	YHF	CPL	YHF	CPL	YHF
W1	Singapore	0	0	1	2	11	15	4	6	1	2
	Seattle	0	0	1	1	8	7	10	12	4	3
	Phoenix	0	0	1	1	6	5	3	4	1	1
W2	Singapore	---	---	---	---	12	11	---	---	---	---
	Seattle	---	---	---	---	9	8	---	---	---	---
	Phoenix	---	---	---	---	4	3	---	---	---	---

Wall	City	Submodel									
		4a		4b		4c		5			
		CPL	YHF	CPL	YHF	CPL	YHF	CPL	YHF		
W1	Singapore	3	10	2	3	20	13	37	59		
	Seattle	2	1	6	8	2	2	16	33		
	Phoenix	4	4	4	7	13	21	204	29		
W2	Singapore	20	23	---	---	---	---	85	30		
	Seattle	11	5	---	---	---	---	18	45		
	Phoenix	7	7	---	---	---	---	124	23		

For submodels 3 and 4, the letters *a*, *b* and *c* indicate that the properties considered constant were evaluated for moisture contents of 0%, 5% and 10%, respectively, for W1, and 0%, 10% and 20%, respectively, for W2. This provided a sensitivity with respect to property variation effects on CPL and YHF. For all cases we used a constant temperature of 25°C to calculate the transport coefficients.

4.1.1 Submodels 1 and 2: omit the source term

First we omitted V_θ , which represents latent specific heat associated with a moisture gradient. We decided to neglect this convection term because the moisture gradient usually has more influence on liquid transport than on vapor transport. We also noticed that, for some materials, $\partial\theta/\partial x$ is small for most wall nodes. The resulting simplification (Submodel 2) gave good results, with percent relative errors below 1% (see Table 4).

Submodel 2 neglects, in addition, V_T ; this means, in effect, that the “pure” and “apparent” thermal conductivities are equal. This is generally true for low temperatures (below 10°C) or low temperature gradients. This Submodel showed a maximum error of 2% in the weekly load for the ACC wall, which is attributable to the fact that the relation D_{TV}/λ is important and the low thermal mass leads to high temperature gradients. However, for wood, this simplification probably would have had larger errors, since D_{TV} is higher; unfortunately, we were unable to analyze wood for this Submodel. For low thermal capacity building elements, where the temperature gradients can be higher, that simplification would have had larger errors as well. One motivation to omit this source term was based on the porous structure. When water released by evaporation leaves a pore or a liquid island, the vapor diffuses through the medium until it encounters a small cavity or liquid island, where it condenses, releasing energy by phase change. As a result, the heat balance is more or less unchanged since the evaporated and condensed portions are roughly equal.

This submodel presented larger errors in hot climates, which is expected since the ratio between the latent and the pure conductivities increases with temperature.

On a 200 MHz Pentium computer, the average run time was 301 seconds using Submodel 0 for the thickest wall (W1) with 37 nodes for one year. Submodels 1 and 2 reduced this time by 19% and 37 %, respectively. The use of more simplified models, such as Submodel 2 can give good results; however, this has to be done with care since the errors can be larger in some situations. For example, in hot and humid climates the temperature gradients and the ratio between the thermal conductivities are both high, which makes this Submodel less accurate in this case.

4.1.2 Submodel 3: omit the source term and assume constant thermal conductivity

The accuracy of the results in this case depends on the value of λ in eq. (10) and $\partial\theta/\partial x$. Basically, these depend on the geometric and thermophysical characteristics of the room envelope, and on the climate and internal conditions. For low moisture content, the “apparent” thermal conductivity is close to the dry thermal conductivity. However, in certain cases, the error caused by assuming λ to be constant can be larger if an incorrect value of θ is used, especially when $\partial T/\partial x$ and $\partial\lambda/\partial\theta$ are large, as for ACC and wood. There is also the problem mentioned above: if the moisture content is high the temperature profile will be delayed relative to the moisture content profile because the thermal mass is higher and the conductivity is constant.

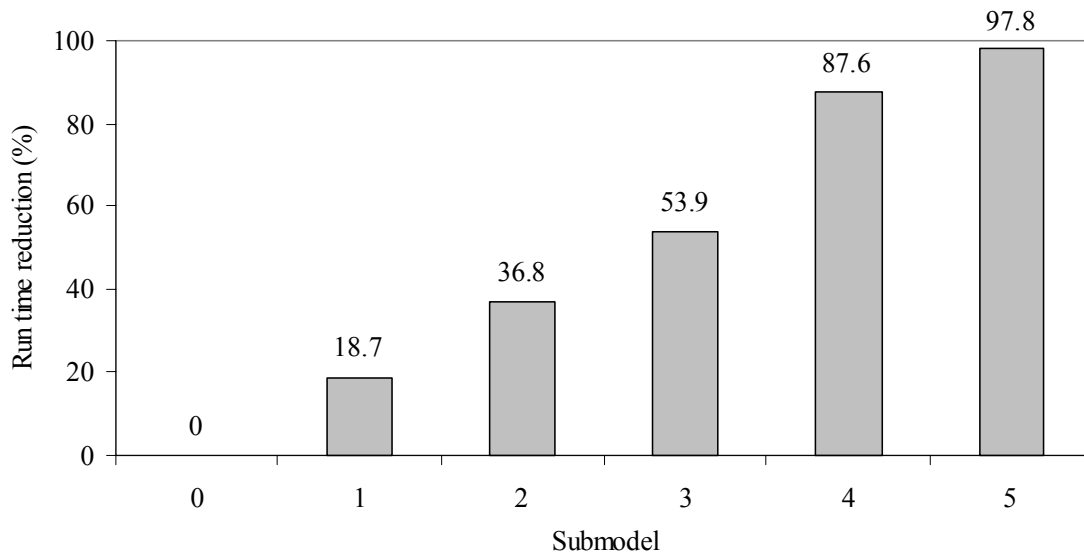


Figure 8: Average reduction in computer run time for different submodels.

Usually, the use of dry-basis conductivity gives rise to higher inaccuracies when the climate is humid for this Submodel, as high moisture content causes a delay between the evolution of temperature and moisture content when compared to drier climates, once the thermal capacity increases and the thermal conductivity is constant. Besides, the moisture dependence of thermal conductivity is high.

Submodel 3, in spite of possessing the above-mentioned problems, leads to results that can, most of the time, be considered good for certain circumstances, such as for calculating YHF in dry climates or when the conduction contribution in porous material is very small compared to other loads such as solar heat gain through fenestration. In those cases, the use of a more sophisticated model is not justifiable and the computer run time reduction should be considered as an important criterion.

Table 4 shows that Submodel 3 can also lead to good results – as low as 1% in the error estimation – when the thermal conductivity is high due to high moisture content, especially for materials for which the thermal conductivity depends strongly on moisture level. For example, in Singapore, the largest difference appeared by using Submodel 3a, as the weather is hot and humid thereby creating high gradients of temperature and moisture content. However, Submodel 3a presented better results for Phoenix, which is much drier (low $\theta(x)$). In Seattle, the wall showed a high moisture content profile (Figure 9) and opposite gradients for temperature and moisture content, so that the effect of high moisture content on the conduction loads was reduced. These moisture effects were also observed for similar cases in Brazil in the cities of Curitiba (Cold/Humid) and Brasília (Hot/Dry) [19].

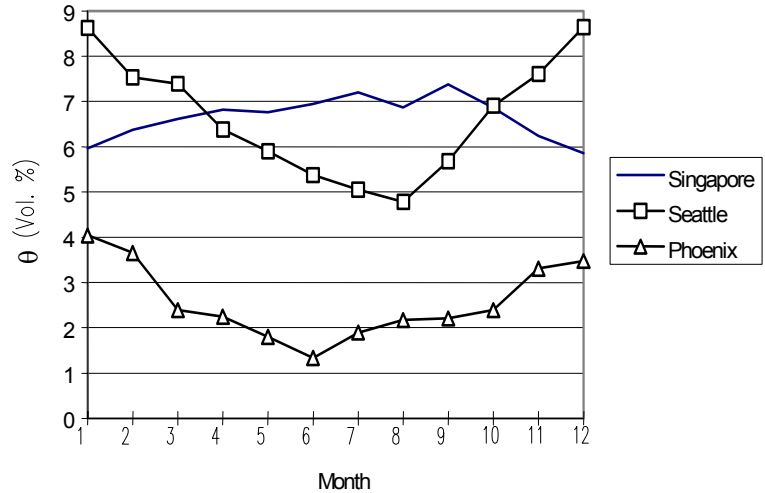


Figure 9: W1 average moisture content in the 3 cities.

Submodel 3c gives precise results (less than 4% relative error) for humid climates since its properties were evaluated for a moisture content of 10%. This content is realistic for mortar, but not for brick; however, the boundary materials have more influence because of both latent conduction and high gradients so that they need a better evaluation of their hygrothermal properties.

In conclusion, neglecting the source term in the energy conservation equation and assuming constant thermal conductivity leads to reasonable results at an average of only 54% of the calculation time of Submodel 0.

4.1.3 Submodel 4: omit the source term assume constant coefficients

Submodel 4 assumes constant coefficients and presents good results when the moisture content gradient is low, which happens for high Biot mass number and low Luikov number [20], making low time and space derivatives for moisture content. The use of this model can be justified when the properties variation is unknown or the governing equation solver does not accept variation on the coefficients. Another factor that can justify the use of this submodel is the program execution rapidness (88% reduction when compared to Submodel 0). It is noticed, through Tab. 4, that submodel 3 has shown better results than submodel 4 for high Luikov number material (W2).

4.1.4 Submodel 5: omit moisture effects

Table 4 shows that the use of Submodel 5 for calculating CPL and YHF usually leads to very large errors, even in the dry Phoenix climate. The main reason for this is that the balance at the wall surfaces completely neglects latent heat exchange.

4.1.5 Conclusion on CPL and YHF sensitivity

Figure 8 gives the average reduction in simulation time for each Submodel. We see that Submodel 4 with constant transport coefficients is almost as fast as Submodel 5, giving results that can be considered satisfactory for certain needs. Figure 9 shows the evolution of W1 average moisture, using Submodel 0, which shows that this wall in Singapore is significantly more humid than in Seattle, except in the months where solar radiation is high, causing large evaporation losses during the day.

It is clear that latent heat plays an important role on the wall energy balance. However, the errors from using Submodel 5 tend to be attenuated once the presence of moisture decreases the temperature due to evaporation, mainly for rooms in which the vapor concentration is low. This reduces the sensible conduction heat transfer calculated with Submodels 0-4, decreasing, therefore, the total conduction heat transfer difference among the models that do and do not consider moisture, especially in hot and humid climates. Unexpectedly, for Phoenix great differences appeared in the calculation of CPL (Table 4), which can be attributed to the fact that phase change at the internal wall surface causes a reduction between the room air and wall surface temperatures, considerably decreasing the instantaneous sensible conduction load. This implies that the maximum conduction heat transfer, calculated by Submodels 0 and 5, occurs at different times. These differences can be even higher when paint is added, as explained in section 4.2.

In general, Submodels 0-4 can be chosen depending on the situation and on the desired accuracy. For example, in a very dry climate, with high sources of thermal load, Submodel 4 can be used with few problems. However, if precise data are available, Submodel 0 or 1 should be used to obtain more reliable results.

4.2 Influence of temperature gradients on moisture diffusion

In this section we evaluate the effect of a temperature gradient on moisture transport, with the goal of obtaining faster submodels that do not need the coefficient D_T , which is difficult to measure.

The analysis is made only for monolithic walls of mortar, wood, brick and aerated cellular concrete in Singapore, since its weather produces high temperature gradients. This sensitivity analysis is done in a similar way to what was done in Section 4.1, verifying the errors by setting $\frac{\partial}{\partial x} \left(D_T \frac{\partial T}{\partial x} \right) = 0$. This hypothesis is applied in the Submodels presented in Section 4.1

(except Submodel 5), renaming them by adding the number 6 followed by original Submodel number. For example, Submodel 6-0 corresponds to Submodel 0 when the moisture migration due to temperature gradients is neglected. Figure 10

The run time reduction is not very significant - around 5% - and, as shown in Figure 10, there may be large errors (up to 40%) depending on the situation, as in the case where the temperature gradient is more important than the moisture content gradient (due to presence of barriers to moisture migration) with a high Posnov number. This simplification should only be used in quasi-isothermal situations or when there is lack of data on D_T , since the run time reduction is insignificant shows the results found under this assumption.

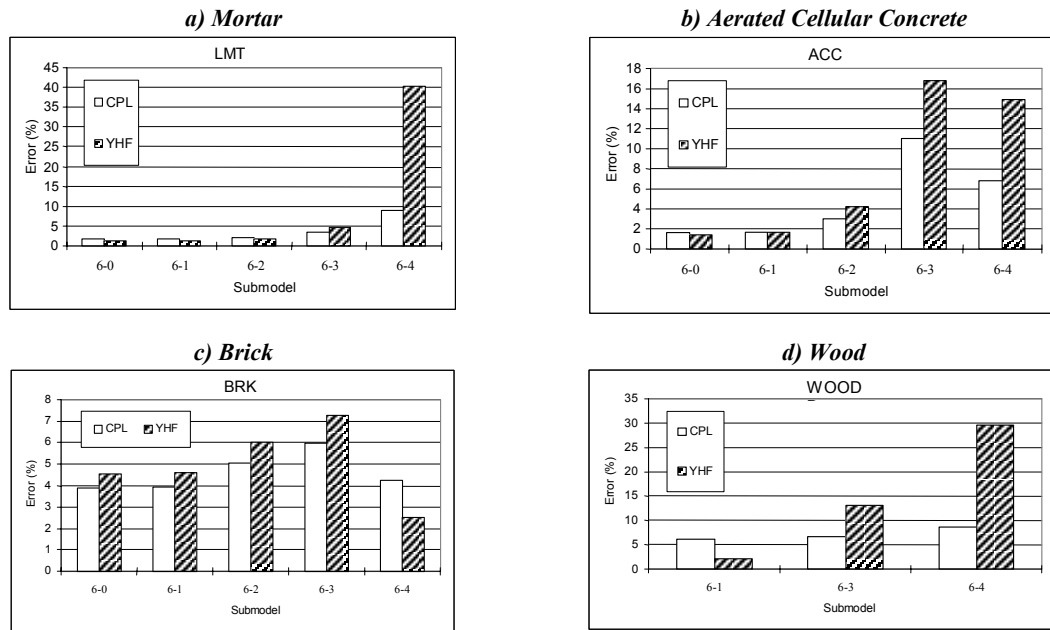


Figure 10: YHF and CPL evaluation error by doing $\frac{\partial}{\partial x} \left(D_T \frac{\partial T}{\partial x} \right) = 0$. a) Mortar; b) Aerated cellular Concrete; c) Brick and d) Wood.

4.3 Paint layer effects

Paint drastically decreases the vapor exchanged between wall surfaces and room air, reducing the latent conduction loads and decreasing the difference among the Submodels. The effect of paint can be included in the convection mass transfer coefficient, h_m , by adding the resistance of the paint layer.

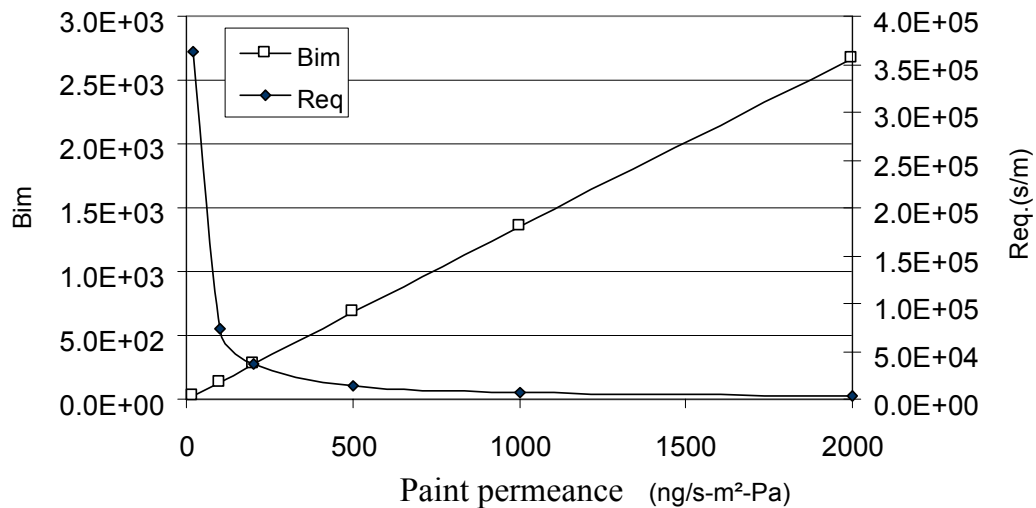


Figure 11: Dependence of Biot mass number (Bi_m) and total vapor resistance (R_{eq}) with the paint layer permeance.

Figure 11 shows values of both Biot mass number and total vapor resistance, R_{eq} , which includes the paint layer resistance. For a wall 0.1m thick we used $h_m = 0.01$ m/s and $D_\theta = 1e-8m^2/s$. We see that R_{eq} decays abruptly with the addition of a paint layer and, for permeances above 500 ng/m²-s-Pa, little variation is noticed. This means that little sensitivity on conduction heat transfer is expected for permeance values higher than a certain value, which is a characteristic of each wall.

For sensitivity analysis we chose paint layer permeance values of 200 and 900 ng/m²-s-Pa, which are close to those used by Rode and Burch [21]. Note that these paints can be placed on the outside or inside of the wall, as shown on Table 5.

Table 5: Permeance values (ng/m²-s-Pa) for 3 different cases.

	Case A	Case B	Case C
External layer	200	900	200
Internal Layer	200	900	900

Figure 11 indicates that even when the permeance is reduced from 900 to 200 ng/m²-s-Pa, the total resistance doesn't increase very much, and, as shown in Table 6, there is little difference among the cases A, B and C. Therefore, although the wall is very sensitive to whether or not it has a paint layer, the effect of the layer is small above a minimum permeance value.

Table 6: Conduction Peak Load (CPL) and Yearly-Integrated Conduction Heat Flux (YHF) estimation errors for W1 with painting (cases A, B and C) in the 3 cities.

Wall	City	Case A		Case B		Case C	
		CPL	YHF	CPL	YHF	CPL	YHF
W1	Singapore	36	11	38	12	38	12
	Seattle	68	55	69	56	69	56
	Phoenix	43	9	43	20	43	19

Table 7 shows that the differences among Submodels 0-4 decrease in average when the moisture content is reduced as it can be seen for Phoenix, except for the CPL estimation by using Submodel 5, which is strongly increased.

It is known that the differences among the Submodels that do and do not consider moisture are due not only to the phase change terms but also due to the variation of thermal conductivity and wall thermal capacity. However, an important parameter is the thermal diffusivity ($\lambda/\rho c$), which tends to become constant with a proportional increase in thermal conductivity and thermal capacity, so that the conduction heat transfer is not really affected in this case.

In order to evaluate the influence of moisture content variation on the thermal capacity and on the thermal conductivity, the following sensitivity coefficients were defined:

$$E_\lambda = \left[\frac{\theta}{\lambda} \frac{\partial \lambda}{\partial \theta} \right]_T \quad \text{and} \quad E_C = \left[\frac{\theta}{(\rho c)} \frac{\partial (\rho c)}{\partial \theta} \right]_T.$$

Figure 12 shows these coefficients for the walls W1 and W2 and, especially for a wood wall, we see that they are quite similar. This can be explained by the fact that the thermal conductivity is affected by moisture as much as the thermal capacity. However, for mortar, it is noticed that for moisture contents higher than 5% the thermal capacity grows much faster than thermal conductivity. Nevertheless, the thickness of the mortar layer in W1 is small, reducing the difference. For wood, the thermal diffusivity, α , is almost independent of moisture content.

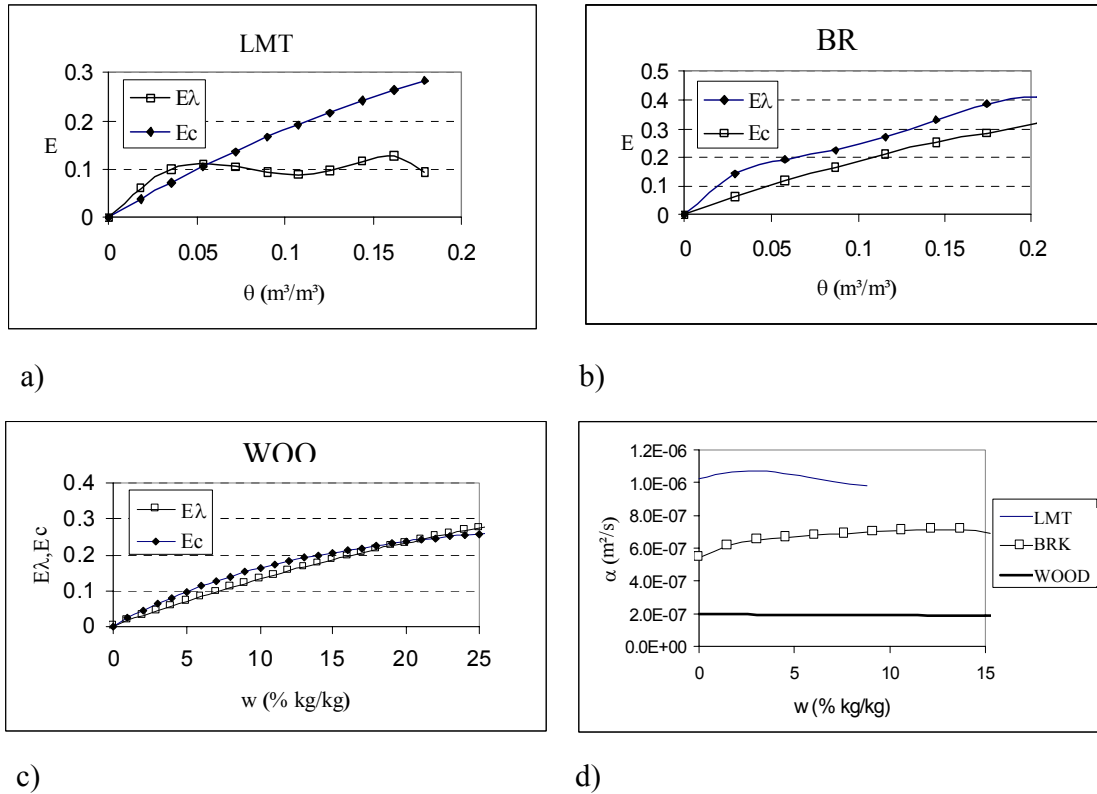


Figure 12: Variation of sensitivity coefficients of thermal capacity and thermal conductivity content with moisture content.

Table 8 compares results of CPL and YHF, with and without painting, vs. results obtained by using Submodel 5. The use of Submodel 5 overestimates CPL and underestimates YHF in all cases. The yearly energy consumption is underestimated, mainly for not adding the latent conduction load to the sensible one. However, in the CPL evaluation, it is noticed that the process of phase change at the internal wall surface induces a reduction in the temperature difference between room air and wall surface, which considerably decreases the instantaneous sensible conduction load. This implies that the peak load, calculated by Submodels 0 and 5, occurs at different time for both Submodels. For example, in Singapore, wall W1 has a conduction heat transfer peak at 5pm on January 27 with Submodel 0 and at 4pm on January 7 with Submodel 5. Comparing Tables 3 and 9 we note that the ratio Q_L/Q_T for the unpainted wall is much higher.

Table 7: Conduction Peak Load (CPL) and Yearly-Integrated Conduction Heat Flux (YHF) estimation errors (in %) for W1 with painting (case C) in the 3 cities.

Wall	City	Submodel									
		1		2		3a		3b		3c	
		CPL	YHF	CPL	YHF	CPL	YHF	CPL	YHF	CPL	YHF
W1	Singapore	0	0	2	3	14	18	8	10	5	7
	Seattle	0	0	1	1	7	5	7	7	3	2
	Phoenix	0	0	1	1	6	5	5	5	2	1

Wall	City	Submodel									
		4a		4b		4c		5			
		CPL	YHF	CPL	YHF	CPL	YHF	CPL	YHF		
W1	Singapore	1	2	0	2	5	8	58	22		
	Seattle	1	1	3	4	1	2	80	9		
	Phoenix	5	4	3	2	7	6	210	10		

Table 8: Comparison of Conduction Peak Load (CPL) and Yearly-Integrated Conduction Heat Flux (YHF) estimation, simulated with

and without painting (case C) in the 3 cities.

Wall	City	Submodel					
		0 (no paint)		0 (paint)		5	
		CPL	YHF	CPL	YHF	CPL	YHF
W1	Singapore	44	23	38	12	60	9
	Seattle	108	76	69	56	124	51
	Phoenix	44	24	43	19	135	17
W2*	Singapore	87	48	59	37	160	33
	Seattle	87	64	61	39	103	36
	Phoenix	91	45	58	41	205	35

* Submodel 0 for wood (W2) means Submodel 1

Table 9: Conduction Peak Load (CPL), maximum latent heat factor $[Q_L/Q_T]_{CPL}$, peak load date, Yearly-Integrated Conduction Heat Flux (YHF) and yearly latent heat factor $[Q_L/Q_T]_{YHF}$ for walls W1 (Submodel 0) and W2 (Submodel 1) in the 3 cities, considering painting (case C).

	W1			W2		
	Singapore	Seattle	Phoenix	Singapore	Seattle	Phoenix
CPL(W/m ²)	38.3	-69.2	43.4	58.5	-61.3	57.9
$[Q_L/Q_T]_{CPL}$	0.10	0.03	0.04	0.10	0.02	0.15
Data (d/m-h) _{CPL}	Jan. 7,5 pm	Dec. 6, 9am	Aug. 1, 5pm	Jan. 7,1pm	Dec. 6, 8 am	Jul. 25, 5pm
YHF (kWh/m ²)	12191.9	-56301	19423	36890	-39480	41106
$[Q_L/Q_T]_{YHF}$	0.15	0.01	0.07	0.08	0.02	0.19

In general, it is noticed that increasing the Biot mass number, by adding a paint layer, causes a reduction in the YHF results obtained among the models that do and do not consider moisture, by decreasing the latent heat flux contribution. On the other hand, for CPL, the difference among Submodels 0 and 5 increases as the latent heat contribution decreases.

It is observed that even in walls with high moisture resistance (in humid or dry climates) it is important to take into account the evolution of the moisture content profile to correctly calculate conduction heat transfer.

The results given in Table 8 suggest that studies should be carried out on energy-efficient walls that take advantage of the coupled heat and moisture transfer phenomenon. For example, the existence of latent heat flux that implies temperature reduction, it would be interesting to allow full evaporation on the external side of the wall so that the conduction heat flux through the wall would be considerably decreased. On the other hand, the internal surface should have a high moisture resistance, reducing both the room air humidity and the latent load. Thus, during the day the most external part of the wall would lose heat by phase change, due to the moisture content rise in the night period. To quantitatively analyze this situation we simulated wall W1 with an infinite permeance paint layer at the outside and a permeance of 100 ng/m²-s-Pa on the inside. This gave a YHF reduction of 11% when compared to the case C, and 54% when compared to the same wall but with no paint on either side.

In a low-energy architecture study, it would be interesting to use a very hygroscopic material on the outside and an impermeable paint layer on the inside, especially in hot and humid climates.

5 CONCLUSIONS

The sensitivity analyses carried out in this work show that simplifications of the full Philip and DeVries model can lead to faster coupled heat and moisture transfer calculations without large loss in accuracy as long as an appropriate value for moisture content is used to evaluate the transport coefficients. The best submodel to use depends on what run time and accuracy are acceptable and on what data are available.

Tables 4 and 8 presented a summary of results of YHF and CLP estimation errors for wall W1 using the different submodels with and without a paint layer. Submodel 1 gave excellent results (0.5% relative accuracy) and did not need information on the coefficient $D_{\theta V}$, which is difficult to measure.

We note Submodel 2 could be included in building simulation programs since it reduces the calculation time by 37% and the accuracy loss is insignificant (< 3%). Submodel 2 is preferable when $D_{\theta V}$ and D_{TV} , which are usually hard to obtain, are unknown. It is also important to note that most of the thermal conductivity values found in the literature are “apparent” since they are easier to be measured than the “pure” values. Thus, Submodel 2 has the advantage of being usable with available material properties; in fact, Submodel 2 becomes Submodel 1 when “apparent” conductivities are used. They are, therefore, possible alternatives to Submodel 0 since they execute in about 1/3 less time and lead to good results.

Submodel 3 uses a thermal conductivity that is considered low for temperature profile calculation, especially in hot and humid climates. However, the latent conduction load determined by this model is nearly precise as the one obtained by Submodel 2, since D_T and D_{\square} are variable and gives a good prediction of moisture content profile, which is not very sensitive to thermal conductivity. Therefore, Submodel 3 errors are due to the underestimated sensible conduction load.

Submodel 4, besides underestimating the thermal diffusivity in the same way that Submodel 3 does, also underestimates the moisture transport coefficients D_T and D_{\square} , leading to a lower moisture content profile and a lower conduction latent load than that calculated by Submodel 3. This reduction of latent load increases the temperature difference between the wall surface and the room air, creating a larger sensible conduction load. Actually, these two effects together are self compensating for the total conduction load calculation (sensible plus latent). In that way, Submodel 4 might evaluate the total conduction load more precisely than Submodel 3, at least for materials with low Luikov number. Nevertheless, Submodel 3 gives more realistic information on the moisture content profile.

Submodels 3 and 4 can be inaccurate in some cases. However, they are far more accurate than Submodel 5. If an accurate conduction calculation is not important, Submodel 4 can be recommended since it fast executing and it requires less material property data. To get accurate results from Submodel 3 or 4 the correct average moisture content must be used, unless there is a vapor barrier and the moisture level is low.

Submodel 4 could be used in building simulation programs that are based on the response factor method (such as DOE-2, BLAST and EnergyPlus) since it requires constant coefficients and is very fast executing (88% run time reduction) and shows good results in terms of heat flux. However, it does not accurately predict the wall moisture content profile, which is important for calculating latent conduction loads and for evaluating mold growth. Using a constant moisture content may overestimate or underestimate the conduction loads. The importance of the correct moisture content for evaluating transport coefficients depends on the material, the weather, and the internal conditions. Some materials, such as brick, have a very low moisture content and gradient, and so are relatively insensitive to what model simplification is used. Also, since brick has high latent conduction loads, the cooling loads increase substantially when moisture is considered.

In conclusion, we have shown the importance of considering moisture in predicting loads through porous walls, even in dry climates when there are paint layers. We have shown that models that ignore moisture may overestimate conduction peak loads up to 210% and underestimate the yearly integrated heat flux up to 59%. This can lead to oversizing HVAC equipment (especially in dry climates) and underestimating energy consumption (primarily in humid climates). Moisture effects can become even more important if internal elements, such as furniture and carpets, are taken into account since they can adsorb significant amounts of moisture at night, which will be released when the air conditioning is turned on, leading to high latent loads.

As our main focus was on the wall, we assumed that room air temperature and relative humidity would not be really affected if we could replace DOE-2 conduction heat transfer model by one of our Submodels 1-5. Thus, we consider valid the use of

DOE-2 as a simulation engine to provide the indoor air conditions. Nonetheless, we are aware that much more work has to be done to perform a whole building hygrothermal simulation analysis.

For further work, we intend to include these heat and moisture transfer models in a whole building simulation program. In this way, it will be possible to quantify the moisture effects on sensible and latent conduction loads by simultaneously solving the building envelope and the air domain in a highly-coupled fashion.

ACKNOWLEDGMENTS

The authors thank CNPq - Conselho Nacional de Desenvolvimento Científico e Tecnológico - of the Secretary for Science and Technology of Brazil and Araucária Foundation of the state of Paraná for support of this work.

NOMENCLATURE

Bi_m	mass Biot number
c	specific heat [J/kg-K].
D_{Tv}	vapor phase transport coefficient associated with a temperature gradient [$m^2/s-K$].
$D_{\theta v}$	vapor phase transport coefficient associated with a moisture content gradient [m^2/s].
D_T	mass transport coefficient associated with a temperature gradient [$m^2/s-K$].
D_θ	mass transport coefficient associated with a moisture content gradient [m^2/s].
h	heat convection transfer coefficient [W/m^2-K].
h_m	mass convection transfer coefficient [m/s].
j	total (vapor plus liquid) flow [kg/m^2-s].
j_v	vapor flow [kg/m^2-s].
L	heat of vaporization [J/kg], wall thickness [m].
q_r	short-wave solar radiation [W/m^2].
T	temperature [$^{\circ}C$].
t	time [s].
x	distance into wall [m].
α	solar thermal radiation absorptance.
λ	thermal conductivity [$W/m-K$].
θ	total moisture volumetric content [m^3 of water / m^3 of porous material].
ρ	mass density [kg/m^3].

Subscripts

app	apparent
l	liquid.
m	mean.
o	solid matrix.
v	vapor.

REFERENCES

- [1] Cunningham M.J., “The Moisture Performance of Framed Structures: A Mathematical Model”, *Building and Environment* 23, pp 123 - 135, 1988.
- [2] Kerestecioglu A. and Gu L., “Incorporation of the Effective Penetration Depth Theory into TRNSYS”, Draft Report, Florida Solar Energy Center, Cape Canaveral, Florida, 1989.
- [3] Burch D.M. and Thomas W.C., “An Analysis of Moisture Accumulation in Wood Frame Wall Subjected to Winter Climate”, NISTIR 4674, Gaithersburg, MD: National Institute of Standards and Technology, 1991.
- [4] El Diasty R., Fazio P. and Budaiwi I., “Dynamic Modelling of Moisture Absorption and Desorption in Buildings”, *Bldg Envir.* 28, pp 21-32, 1993.
- [5] Liesen, R.J., “Development of a Response Factor Approach for Modeling the Energy Effects of Combined Heat and Mass Transfer with Vapor Adsorption in Building Elements”, Ph.D. thesis, Mechanical Engineering Department, University of Illinois, 1994.
- [6] Yik F.W.H., Underwood C.P. and Chow W.K., “Simultaneous Modelling of Heat and Moisture Transfer and Air-conditioning Systems in Buildings”, *Proc. IBPSA Building Simulation '95*, 4th International Conference, Madison, WI, USA, 1995.
- [7] IEA (International Energy Agency) Annex 24 Final Report, Heat, Air, and Moisture Transfer in Insulated Envelope Parts, Vol 1, Task 1: Modelling, Belgium, 1996.
- [8] Rode C. and Burch D.M., *Empirical Validation of a Transient Computer Model for Combined Heat and Moisture Transfer, Thermal Envelopes VI*, 1995.
- [9] De Freitas V.P., Abrantes V., Crausse P., *Moisture Migration in Building Walls – Analysis of the Interface Phenomena*, *Building and Environment*. 31, No. 2, pp. 99-108, 1996.
- [10] Philip, J. R. and De Vries, D. A., “Moisture movement in porous materials under temperature gradients”, *Transactions of the American Geophysical Union*. v.38, n.2, p.222-232, 1957.
- [11] Mendes N., Philippi P.C. and Lamberts R., *A New Mathematical Method to Solve Highly-Coupled Equations of Heat and Mass Transfer in Porous Media*, *International Journal of Heat and Mass Transfer*, Vol. 45/3, pp. 509-518, 2002.
- [12] Winkelmann F. C., Birdsall B. E., Buhl W. F., Ellington K. L., Erdem A. E. DOE-2 Supplement, V. I, Version 2.1E, Energy and Environment Division. Lawrence Berkeley Laboratory. University of California, Berkeley, CA, 1993.
- [13] Winkelmann F. C., Birdsall B. E., Buhl W. F., Ellington, K. L., Erdem A. E. DOE-2 Supplement, V. II, version 2.1E, Energy and Environment Division. Lawrence Berkeley Laboratory. University of California, Berkeley, CA, 1993.
- [14] Mendes N. and Philippi P.C., *Heat and Moisture Transfer Model Through the Interface between Porous Media of Different Hysteresis*, *Brazilian Conference on Engineering and Thermal Science (ENCIT 2002)*, Caxambu-MG, Brazil, 2002. (in Portuguese)
- [15] Patankar S.V., *Numerical Heat Transfer and Fluid Flow*, McGraw-Hill, 1981.
- [16] Perrin, B., “Etude des transferts couplés de chaleur et de masse dans des matériaux poreux consolidés non saturés utilisés en génie civil”, *Thèse Docteur D'Etat*, Toulouse, Université Paul Sabatier de Toulouse, 1985. 267p.
- [17] Siau J.F., “*Transport Processes in Wood*,” Springer-Verlag, New York, 1984.
- [18] Cunha Neto, J. A. B., *Transport d'humidité em matériau poreux en présence d'un gradient de température. Caractérisation expérimentale d'un béton cellulaire*. Thèse de Docteur, 194p, Grenoble, Université Joseph Fourier - Grenoble I, 1992.
- [19] N. Mendes, R. Lamberts and P.C. Philippi, *Moisture Migration Through Exterior Envelopes in Brazil*, *ASHRAE Transactions*, 2002. (In Press)

[20] Mendes N., Models for prediction of heat and moisture transfer through porous building elements, Ph.D. Thesis, 225p., Federal University of Santa Catarina - UFSC, Florianópolis - SC, Brazil, 1997. (In Portuguese).

[21] Rode C. and Burch D.M., Empirical Validation of a Transient Computer Model for Combined Heat and Moisture Transfer, pp. 283-295, ASHRAE transactions, 1995.

LIST OF TABLES

Table 1: Schematic description of the Submodels derived.

Table 2: Dry-basis material properties for lime mortar.

Table 3: Conduction Peak Load (CPL), maximum latent heat factor $[Q_L/Q_T]_{CPL}$, peak load date/hour, Yearly-Integrated Conduction Heat Flux (YHF) and yearly latent heat factor $[Q_L/Q_T]_{YHF}$ for walls W1 (Submodel 0) and W2 (Submodel 1) in the 3 cities.

Table 4: Conduction Peak Load (CPL) and Yearly-Integrated Conduction Heat Flux (YHF) estimation errors in Singapore, Seattle and Phoenix, compared to Submodel 0 (Submodel 1 for W2).

Table 5: Permeance values (ng/m²-s-Pa) for 3 different cases.

Table 6: Conduction Peak Load (CPL) and Yearly-Integrated Conduction Heat Flux (YHF) estimation errors for W1 with painting (cases A, B and C) in the 3 cities.

Table 7: Conduction Peak Load (CPL) and Yearly-Integrated Conduction Heat Flux (YHF) estimation errors for W1 with painting (case C) in the 3 cities.

Table 8: Comparison of Conduction Peak Load (CPL) and Yearly-Integrated Conduction Heat Flux (YHF) estimation, simulated with and without painting (case C) in the 3 cities.

Table 9: Conduction Peak Load (CPL), maximum latent heat factor $[Q_L/Q_T]_{CPL}$, peak load date, Yearly-Integrated Conduction Heat Flux (YHF) and yearly latent heat factor $[Q_L/Q_T]_{YHF}$ for walls W1 (Submodel 0) and W2 (Submodel 1) in the 3 cities, considering painting (case C).

LIST OF FIGURES

Figure 1: Internal and external temperatures in Singapore.

Figure 2: External and internal relative humidities in Singapore.

Figure 3: Incident solar radiation on the south facade for Singapore and on the north facade for Seattle.

Figure 4: Mass transport coefficients for lime mortar

Figure 5: Mass transport coefficients for brick

Figure 6: Thermal conductivity for brick and lime mortar.

Figure 7: Sorption isotherms curves for brick and lime mortar.

Figure 8: Average reduction in computer run time for different submodels.

Figure 9: W1 average moisture content in the 3 cities.

Figure 10: YHF and CPL evaluation error by doing $\frac{\partial}{\partial x} \left(D_T \frac{\partial T}{\partial x} \right) = 0$. a) Mortar; b) Aerated cellular Concrete; c) brick and d)

Wood.

Figure 11: Dependence of Biot mass number (Bi_m) and total vapor resistance (R_{eq}) with the paint layer permeance.

Figure 12: Variation of sensitivity coefficients of thermal capacity and thermal conductivity content with moisture content.